FIV2024
IGUAÇU FALLS, BRAZIL
2-5 JULY 2024

FIV2024: FSI² & FIV + N
10th International Symposium on Fluid-Structure Interactions,
Flow-Sound Interactions, Flow-Induced Vibration & Noise

FIV2024-0119
Exploring the VIV phenomenon through a coupling between rigid-body and flexible modes

Aline Leal de Lima Gontarski [1]
aline.peresleal@usp.br
Guilherme Rosa Franzini [1]
gfranzini@usp.br
André Luis Condino Fujarra [2]
andre.fujarra@ufsc.br
Celso Pupo Pesce [1]
ceppesce@usp.br

[1]Offshore Mechanics Laboratory, Polytechnic School of the University of São Paulo
[2]Fluid-Structure Interaction Laboratory, Technical Center of Joinville, Federal University of Santa Catarina

Abstract. *Vortex-induced vibration (VIV) in flexible cylinders typically exhibits the coexistence of several natural modes. This work explores a deeper understanding of coupled VIV responses, reaching details of how nonlinear and complex dynamics depend on nondimensional control parameters. The experimental setup comprises a flexible cylinder of* $0.7m$ *in length, with external diameter, aspect ratio, and mass ratio of* $D = 25mm$, $L/D = 28$ *and* $m^* \approx 4.5$, *respectively, which is vertically cantilevered from a leaf spring support of one degree of freedom with natural frequency controlled by changing its spring stiffness. Through this assembly, it is possible to investigate the modal coexistence due to VIV when the natural frequency of the rigid body is appropriately calibrated to values close to the first two natural frequencies of the flexible cylinder. These conditions were investigated for a wide range of 20 reduced velocities. For measurement purposes, a motion capture system records rigid body dynamics, while four inertial measurement units (IMUs) placed inside the flexible cylinder are used to record acceleration and rotational rate data during testing. A signal processing procedure has been developed and applied to transform accelerations into displacements along the flexible cylinder, which is a complete reference framework for the analysis of simultaneously excited VIV responses. In this sense, frequencies and nondimensional amplitudes are evaluated during the tests, obtained based on the application of Fourier and Hilbert-Huang transforms. The results provide information that contributes to the improvement of the theoretical models currently used for prediction of coupled VIV responses, particularly as regards the interdependence between natural modes in relation to the reduced velocity that has excited them. The results also contribute to an interesting discussion of the subject.*

Keywords: *VIV, modal coexistence, flexible cylinder, leaf spring support, IMU.*

1. INTRODUCTION

Flexible structures such as cables, beams, and risers demonstrate a multimodal response when exposed to external harmonic or periodic excitation. Enhanced responses become noticeable when the excitation frequency is close to any of the natural frequencies of the system. This leads to the presence of several resonance ranges of flow velocity marked by modal co-existence, highlighting the intricate and detailed aspects of the structural response.

Vortex-induced vibrations (VIV) are a self-induced and self-controlled phenomenon that occurs in slender structures, where vortices shed from the body induce periodic oscillations.

The VIV response of rigid structures mounted on elastic supports, specifically cylinders, has been fundamentally investigated by Khalak and Williamson (1999); Govardhan and Williamson (2000); Williamson and Govardhan (2004), showing upper and lower branches in the VIV curve.

For flexible cylinders, the VIV response is characterized by a higher level of complexity in its details. As illustrated in Pesce and Fujarra (2000, 2005), additional response branches can emerge, which requires more advanced instrumentation for data acquisition along the structural length, as well as a specific methodology for data analysis, including modal decomposition and methods to assess phase differences. Research on the response of flexible cylinders has been explored from various perspectives, using an analytical approach, computational fluid dynamics (CFD), and experimental methods to assess multiple dynamic scenarios. It is important to note that the VIV response is influenced by various parameters such as the oscillating mass, bending stiffness, damping coefficient, Reynolds number, and boundary conditions.

In the context of displacements imposed on the top of the cylinder, resulting in parametric excitation, Franzini *et al.*

(2015) employed vertical and specified monochromatic harmonic movements on the top of a partially submerged flexible cylinder, causing variations in natural frequencies. The presence of the prescribed top motion resulted in an increase in the maximum oscillation amplitude from 0.7 diameters to a value slightly larger than one diameter, as observed in the case $f_t : f_{N,1} = 1 : 1$. The paper of Franzini *et al.* (2016) investigates the concomitant excitation of VIV and axial motion in a vertical and flexible cylinder. Experiments reveal that top-motion excitation at $f_t : f_{N,1} = 2 : 1$ enhances cross-flow vibrations and broadens Fourier spectra at high reduced velocities. On the contrary, the top motion at $f_t : f_{N,1} = 3 : 1$ results in different response frequencies and modulation of the amplitude. Modal amplitude time histories show that parametric excitation at $f_t : f_{N,1} = 2 : 1$ doubles the characteristic oscillation amplitude, while at the ratio $f_t : f_{N,1} = 3 : 1$, amplitudes decrease at lower reduced velocities and remain comparable at higher velocities.

To the best of the authors' knowledge, only a limited number of experimental studies have specifically examined the effects of stiffness modulation on the VIV response. Modulating the top excitation by frequencies, Pesce *et al.* (2006) discusses the application of the Hilbert-Huang spectral analysis method to analyze these complex VIV behaviors. To illustrate the application of the method, one of the experimental cases was with a leaf spring that held a flexible rubber cylinder, restricting the vibrations of the body to the transverse motion. The sub harmonic resonance mode presented large transverse amplitudes and followed a branch that merges with the usual lower branch response. In the study conducted by Franzini *et al.* (2008), a new electrically driven movable spring-leaf system is introduced to address elastic-mounted cantilevered cylinders, whether rigid or flexible. Research presents results for rigid cantilevered cylinders mounted on this innovative apparatus, examining entire VIV responses, including amplitude and frequency curves in relation to reduced velocity. The apparatus used in the current analysis is identical and comprises an elastic leaf-spring base with variable leaf-spring span. The span can be controlled by a conventional electric system, specifically a step-driver motor. The VIV results in Franzini *et al.* (2014) consider a flexible clamp-free cylinder simultaneously tested with a rigid cylinder elastically supported. The study employs two analytical approaches based on accelerometer data: a standard statistical method and the Hilbert–Huang spectral analysis technique (HHT). The results reveal that the rigid cylinder exhibits classical initial, upper, and lower branches, while the flexible clamped-free cylinder displays a distinctive super-upper branch in its response. This comparative analysis provides fundamental insights into the complex dynamics of VIV for different structural configurations.

Taking into account different effects of nonlinear interaction, the main objective of this study is to conduct a thorough investigation into the dynamics of a flexible cylinder installed on a flexible base, combining movements of both rigid and flexible bodies. The investigation covers the analysis of the response curve VIV for the rigid cylinder on the elastic base in three stiffness values. Then, the flexible cylinder is evaluated in clamped-free condition and in the elastic base with two different stiffness: near the first flexible natural frequency (0.6Hz) and between first and second natural frequencies (1Hz). Amplitudes, frequencies, and movement phases are compared to explore the dynamic response when coupling rigid-body and flexible modes.

Section 2.provides comprehensive details on rigid and flexible models, the leaf spring apparatus, data acquisition systems, and a description of the tests carried out. Section 3.presents the signal processing used with the measurement units and the calculation of important parameters. Section 4.presents the VIV results of the rigid body and flexible cylinder, with a discussion of the dynamics of coupling between the natural modes of vibration. Finally, Section 6.provides an overview of the conclusions drawn from the experiments.

2. EXPERIMENTAL SETUP

2.1 Rigid and flexible cylinders and the leaf spring support

The rigid cylinder has an external diameter of $D = 25mm$ and a total length of $L = 700mm$. The mass ratio, which relates the vibrating mass to the displaced mass in the fluid, is $m^* \approx 4$.

The flexible cylinder is made up of silicone rubber and stainless steel microspheres, which form a composite material. It has an external diameter of $D = 25mm$, an aspect ratio of $L/D = 28$, and a mass ratio of $m^* \approx 4.5$, which is similar to that of the rigid cylinder; see Fig. 1. The adaptable design was created to accommodate inertial measurement units, particularly the HW-290 module, which measures $18mm$ in width. Static tests were conducted to assess the bending stiffness by adjusting the span length in balance and determining the static deflection.

Both cylinders were vertically supported as cantilevers by a leaf spring support in individual test sessions. The leaf spring support is a variable-span leaf spring system created to support cantilevered cylinders and generate vibration only in the cross-wise direction. In this research, three values of the vertical leaf spring length were employed to attain a particular stiffness which helped establish the natural frequency of the system in the crosswise direction. The leaf spring support can be seen in Fig. 2.

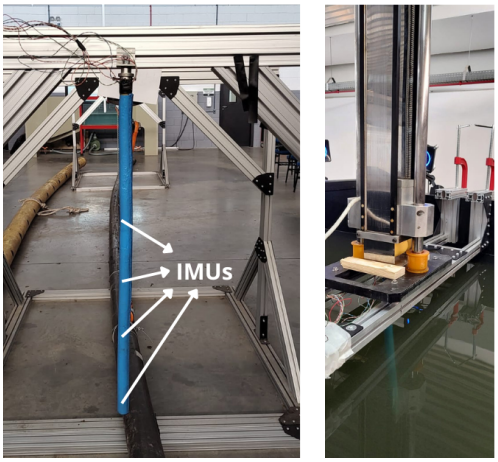

Figure 1. Flexible model in air illustrating the IMUs positions (left) and, flexible cylinder placed in water, in the clamped-free condition (right).

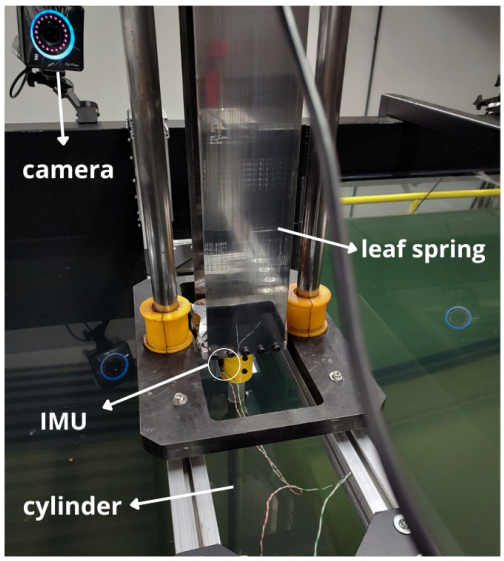

Figure 2. Experimental setup for the rigid cylinder in the leaf spring support.

2.2 Channel facility and measurement systems

The experiments were carried out in the circulating water channel (CWC) of the Federal University of Santa Catarina (UFSC), which is $1400mm$ wide and $1200mm$ deep; see Fig. 3.

The reduced velocity for each test was determined based on the flow velocities at the CWC, as follows:

$$Vr = \frac{U}{f_{ny}D}, \tag{1}$$

where U is free-stream velocity, D is the cylinder diameter and f_{ny} is the first natural frequency of the flexible cylinder. To obtain the natural frequencies for each condition, decay tests were performed in air and still water.

Three cameras were set in the framework above the channel for the optical tracking system, called OptiTrack. This system collects data only in air, that is, the displacement of the leaf spring support. However, in the absence of underwater cameras, the tracking system used to monitor the inline and cross-flow responses of the flexible cylinder was based on inertial measurement units (IMUs).

The IMUs use the inertial principle to give information related to acceleration of the body, using gravitational acceleration as a reference, and rotation rate, using conservation of momentum. The low-cost IMUs used in the present work basically comprise 3 accelerometers, 3 rate gyros, and a magnetometer. Then, it is necessary to perform proper signal processing to obtain reliable data about the required quantities (inline and cross-flow displacements). To validate the data collected from the IMUs, measurements of the upper IMU, the one installed on the leaf spring support, were compared with those obtained by the optical tracking system.

In the VIV analysis, it is crucial to assess the movements in both directions, as well as the respective frequencies of vibration, particularly in relation to the multi-modal excitation. The procedure for handling the signals to achieve this is described in Section 3.

2.3 Decay and VIV experiments

Experiments were conducted to assess the motions of rigid and flexible bodies using cylinders with comparable properties.

Based on the MEF calculations, frequencies equal to 0.6, 1 and $1.5Hz$ were defined as appropriate to determine the lengths of the leaf springs. These frequencies are close to the first natural mode of the flexible cylinder and between the second and third modes for the flexible cylinder mounted on the leaf spring support, as can be seen in Tab. 1. These frequencies also took into account the limitation of the length of the leaf spring support and the CWC velocities.

Using the rigid cylinder, it was possible to determine the stiffness generated by the leaf spring support and generate the VIV response curve for the movement of its pure translation. This condition was evaluated through three lengths of leaf springs to obtain the natural frequencies shown in Tab. 1. The VIV tests using each leaf spring condition with the rigid cylinder are identified in Tab. 1 as Cases 01, 02 and 03.

Subsequently, the flexible cylinder was subjected to a modal identification procedure. Through decay experiments, the clamped-free condition was tested, and it was possible to determine the first three natural frequencies (similar in both directions due to the cylinder symmetry), presented in Tab. 1 for the corresponding boundary condition. The VIV test in this same boundary condition with the flexible cylinder is named Case 04.

Then, the two lengths of the leaf springs corresponding to 0.6 and $1Hz$ were used to perform VIV tests with the flexible cylinder attached to the leaf spring support, named Cases 05 and Case 06, respectively.

The modal shapes for Cases 1-6 are illustrated in Fig.4, obtained by simulations of the finite element method (FEM). For the rigid cylinder attached to the elastic support, Fig.4 (a, b, and c), only cross-flow deformation is observed. For the clamped-free flexible cylinder, Fig.4 (d, e, and f), the modes are symmetric. For the flexible cylinder attached to the elastic support, Fig.4 (g to l), the first and third modes are in the cross-flow direction, considering the elastic base and the flexible moving, while the second mode is related to the movement only of the flexible in the inline direction.

Through this series of experiments, the IMU measurements were validated, the natural frequencies and damping factors were identified, and the VIV responses were determined accordingly.

Name	Cylinder	f_1, Hz	f_2, Hz	f_3, Hz	Boundary condition
Case 01	rigid	0.64	-	-	Elastic base
Case 02	rigid	0.99	-	-	Elastic base
Case 03	rigid	1.45	-	-	Elastic base
Case 04	flexible	0.58	2.16	5.24	Clamped-free
Case 05	flexible	0.50	0.71	1.18	Elastic base
Case 06	flexible	0.50	0.71	1.40	Elastic base

Table 1. Parameters of each test .

Figure 3. Circulating water channel facility at UFSC.

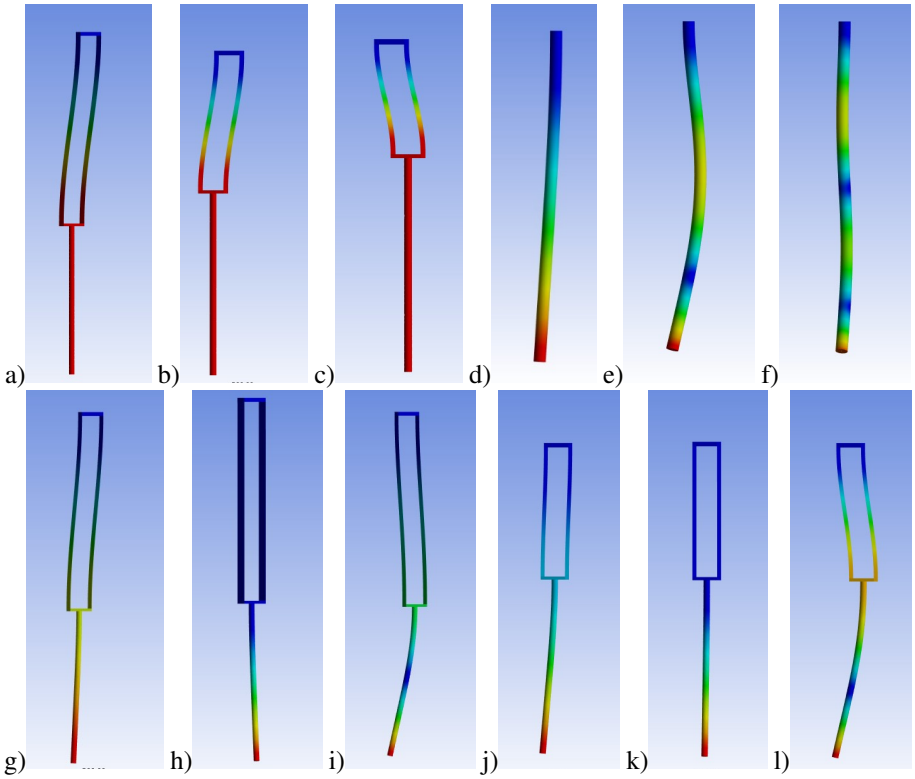

Figure 4. Modal shapes a) First mode Case 01, b) First mode Case 02, c) First mode Case 03, d) First mode Case 04, e) Second mode Case 04, f) Third mode Case 04, g) First mode Case 05, h) Second mode Case 05, i) Third mode Case 05, j) First mode Case 06, k) Second mode Case 06, l) Third mode Case 06.

3. SIGNAL PROCESSING

Regarding signal processing, the initial stage involved handling the raw data received from the IMUs. Calibration was conducted before the decay and VIV experiments, collecting data to calculate offsets and gain for the accelerometers, rate gyros, and magnetometers.

Using static readings at different positions and gravitational acceleration as a reference, the accelerometers were calibrated. The rate gyros follow the same way, but the constant readings were collected and calibrated using the precise positioning system of a CNC machine. Magnetometers, on the other hand, need to take into account the magnetic field around them, and it is necessary to obtain data from the environment considered. The magnetic measurement, when error-free, shall display a zero-centered reading sphere. When the magnetic field experiences disruption, hard iron distortions cause a consistent bias that persists in magnetic measurements over time, shifting the center of the sphere. Soft-iron distortions, on the other hand, alter and deform the preexisting magnetic fields, making it an ellipsoid.

Next, Euler angles are calculated by the following relations:

$$\phi = \tan^{-1}\left(\frac{-a_{c,y}}{-a_{c,z}}\right) \tag{2}$$

$$\theta = \tan^{-1}\left(\frac{a_{c,x}}{\sqrt{a_{c,y}^2 + a_{c,z}^2}}\right) \tag{3}$$

where a_c is the acceleration component in x, y or z directions in object (IMU) frame.

The yaw angle could not be computed only with accelerometers and needs the magnetometers readings as follows:

$$\psi = \tan^{-1}\left(\frac{M_Y}{M_X}\right) \tag{4}$$

being:

$$\begin{aligned} M_Y &= -m_{c,y}\cos\phi + m_{c,z}\sin\phi \\ M_X &= m_{c,x}\cos\theta + m_{c,y}\sin\phi\sin\theta + m_{c,z}\cos\phi\sin\theta \end{aligned} \tag{5}$$

where the readings are on the axis x, y and z of the object frame.

Angles calculated by the IMU refer to the Earth frame, or fixed frame. To evaluate the results in a defined reference frame, it is necessary to know the angles of this reference and perform a final rotation. Assuming that the reference frame aligns with gravity, the only angle that needs to be rotated is the yaw to align the in-line and cross-flow directions. Details about the IMU signal processing can be found in Fujarra *et al.* (2023).

As the accelerations were acquired, the corresponding displacements were calculated through double integration in the frequency domain, within the specified reference frame, characterized by the following procedure:

$$\iint_{-\infty}^{\infty} y(t)dt = \text{IFFT}\left\{\frac{y(f)}{(j2\pi f)^2}\right\} \tag{6}$$

considering the frequency bandwidth of interest.

Significant displacement amplitudes were determined through standard statistical analysis, with the Root Mean Square (RMS) amplitude serving as an effective metric to characterize the signal's amplitude over time. The normalized RMS amplitude was computed as follows.

$$A^{rms}/D(X) = \frac{1}{D}\sqrt{\frac{1}{N}\sum_i X(i)^2} \tag{7}$$

and the the maximum significant amplitude is represented by:

$$A/D = \sqrt{2}A^{rms}/D \tag{8}$$

The frequency spectrum was calculated using the Fast Fourier Transform (FFT), an algorithm to compute the discrete Fourier transform (DFT). From the decay tests the natural damped frequency is considered as the peak frequency in the spectrum and, the damping factor ζ was computed by logarithm decrement:

$$\delta = \frac{1}{\pi} log\left(\frac{x_n}{x_{n+1}}\right) \tag{9}$$

$$\zeta = \frac{\delta}{\sqrt{(4\pi^2 + \delta^2)}} \tag{10}$$

The instantaneous angle phase difference was computed by the Hilbert-Huang transform (HHT), as follows:

$$\psi_{phase} = \tan^{-1}\left(\frac{Im\{\text{HHT(t)}\}}{Re\{\text{HHT(t)}\}}\right) \tag{11}$$

4. RESULTS

4.1 Experimental VIV results for the rigid cylinder

The rigid cylinder fixed to the leaf spring support was characterized by decay tests in still water. The natural damped frequencies experimentally obtained were $f_1^r = 0.64Hz$, $f_2^r = 0.99Hz$, and $f_3^r = 1.45Hz$.

The root mean square amplitudes of displacement at the reduced velocities for three leaf-spring stiffness are illustrated in Fig.5. The representation related to the natural frequency of the respective stiffness of the leaf spring support ($Vr = U/(f_{n,Case}D)$) shows a similar behavior for the lock-in range, quickly reaching the peak amplitude (0.6D) and decreasing in two stages, the upper and lower branches. The difference is related to the decreasing stage, where the position with the fastest frequency presents a broader curve with a lower slope. With the curves built over the natural frequency of Case 01 ($Vr = U/(f_{n,Case01}D)$), it is possible to note the resonance regions for a body with multiple natural frequencies. In the last case, the curves overlap, which might modify the behavior of the multimodal oscillation.

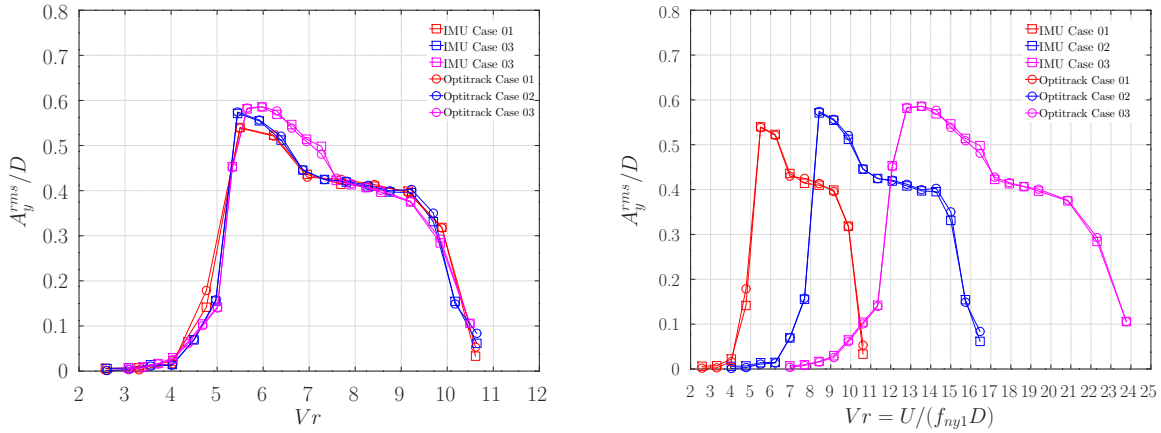

Figure 5. RMS amplitudes in the cross-flow direction for the rigid cylinder in the leaf spring apparatus. Reduced velocity computed according to each natural frequency (left) and computed with the first natural frequency (right).

5. Experimental results for the flexible cylinder

Following, the flexible cylinder was tested. The natural damped frequencies obtained experimentally were $f_1^f = 0.58Hz$, $f_2^f = 2.16Hz$ and $f_2^f = 5.24Hz$. The typical damping factor was $\zeta = 3.3\%$, given a product $\zeta m^* = 0.15$. The process of obtaining the damping factor is illustrated in Fig.6.

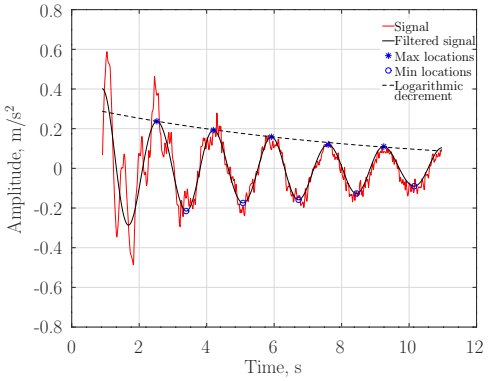

Figure 6. Acceleration decay in water, for the cross-flow direction.

For the clamped-free condition, significant cross-flow amplitudes are shown in Fig.7. The amplitudes are represented in terms of the respective IMUs placed along the flexible cylinder. In particular, the amplitudes are higher at the end of the cylinder. Two regions of higher amplitudes are identified for reduced velocities close to $Vr = 7$ and $Vr = 23$, corresponding to the first and second natural frequencies, respectively. These oscillation frequencies are confirmed in the frequency spectrum with $f_y/f_{ny} \approx 1$ and $f_y/f_{ny} \approx 3$, respectively. For $Vr > 16$ it is possible to see traces of the first and second frequencies, but the second mode ends up predominating in the VIV response.

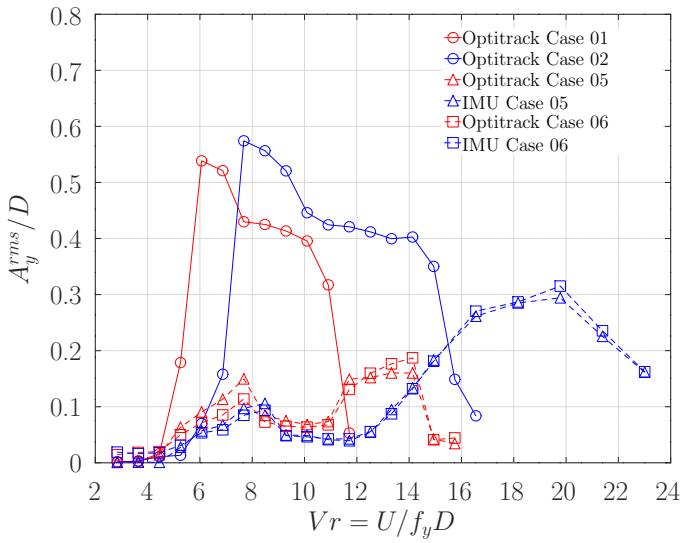

Figure 8. RMS amplitudes for the leaf spring apparatus with the rigid (Cases 01 , 02 and 03) and flexible cylinder (Cases 05 and 06).

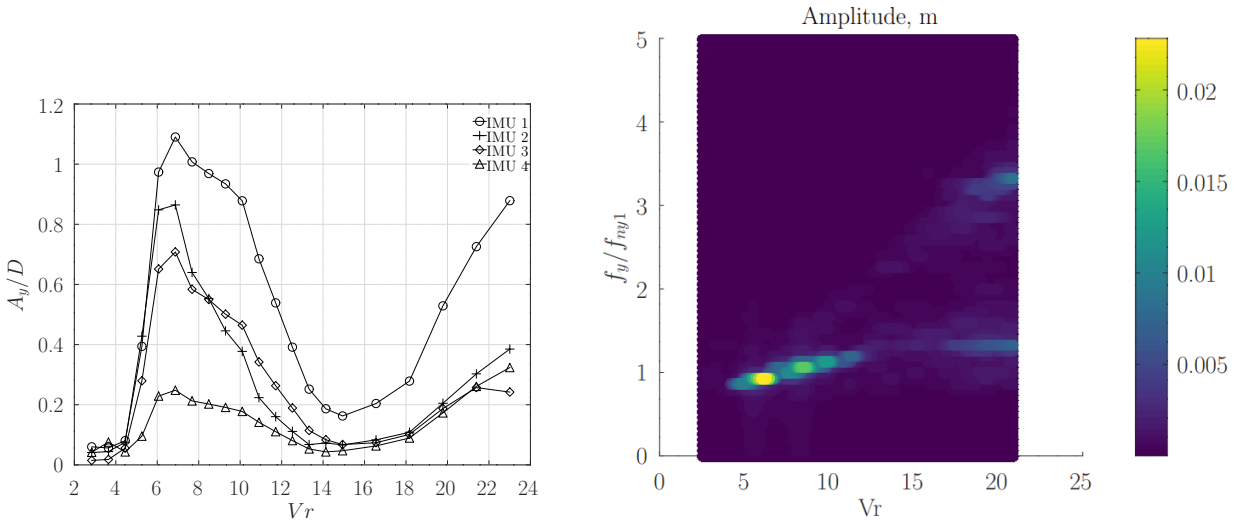

Figure 7. Results for the flexible cylinder in the in the clamped-free boundary condition. RMS of cross-flow amplitudes (left) and frequency spectra from the IMU 1 (right).

For the next configuration, where the flexible cylinder is fixed in the leaf spring support, the first analysis is related to the leaf spring movement itself. The results are shown for the IMU and optical tracking systems; see Fig. 8; compared with the case of the rigid cylinder. When the flexible cylinder is attached to the support, its response amplitudes drastically decrease.

For the position where the leaf spring has a natural frequency of $0.6Hz$, Case 05, the red lines in Fig.8, the first synchronization occurs in $6 < Vr < 9$ with a maximum rms amplitude of $0.15D$ and frequencies close to $0.5Hz$. A second region appears in $11 < Vr < 15$, the peak frequency in this case is $\approx 1.2Hz$. The response frequencies related to the first natural frequency of the flexible can be seen in Fig. 9, with frequency ratios near one for the first region and near two for the second region.

For Case 06, where the leaf spring was placed in the position corresponding to $1Hz$, the blue lines in Fig. 8, amplitudes change. The same first synchronization region occurs, with lower amplitudes and oscillation frequency of $0.5Hz$. The second synchronization occurs in $15 < Vr < 23$, with a maximum rms amplitude of $0.3D$ vibrating at about $1.4Hz$.

It should be noted that the response to the leaf spring is altered by the flexible body. For low velocities, the flexible body seems to control the response. For high velocities, new natural frequencies appear for the whole system.

Analysis of the flexible cylinder mounted on the leaf spring reveals the maximum amplitudes for the flexible body as depicted in Figure 10. The values for the clamped-free and with two leaf spring positions are compared. When the movements of rigid and flexible bodies are coupled, the amplitudes are larger, mainly at the resonance peak, where the

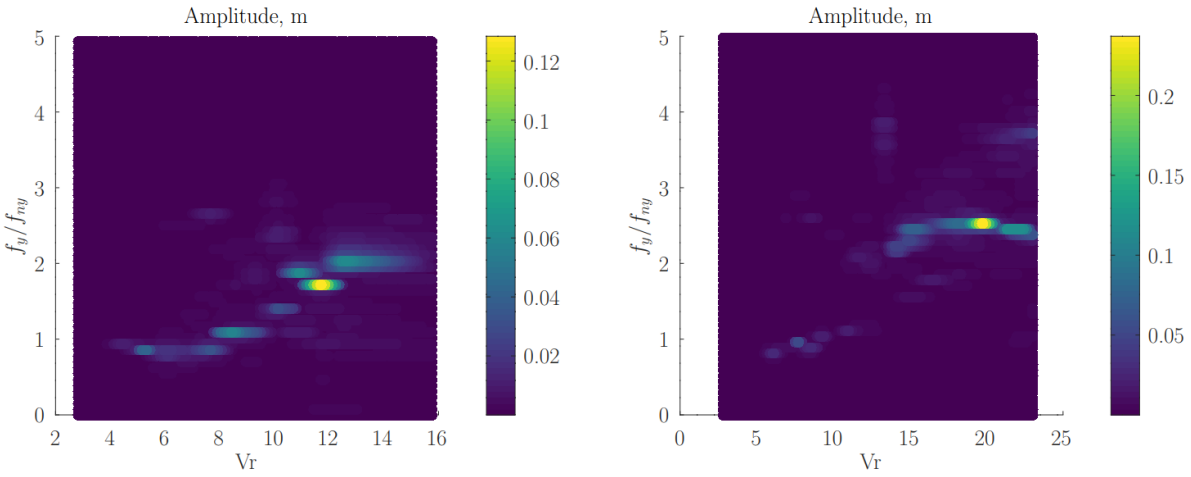

Figure 9. Frequency spectra for the leaf spring apparatus at position 0.6Hz (left) and 1Hz (right) with the flexible cylinder.

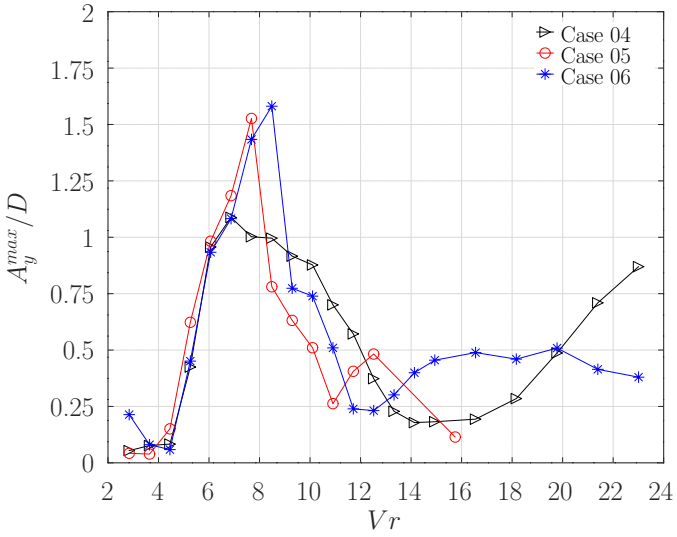

Figure 10. Maximum cross-flow amplitudes for the flexible cylinder in three different boundary conditions: clamped-free(Case 04), leaf spring at 0.64Hz (Case 05) and, leaf spring at 0.99Hz (Case 06).

cross-flow amplitudes are $> 1.5D$, showing the upper branch Pesce and Fujarra (2000, 2005). The decreasing stage is also faster, not appearing the lower branch.

For Case 05, two synchronization regions appear, with frequencies 0.5 and $1.2Hz$, corresponding to the first and third modes, respectively, of the system composed of the flexible cylinder mounted on the leaf spring support. For Case 06, even with higher velocities, only two synchronization regions appear, with frequencies 0.5 and $1.4Hz$, again related to frequencies for the whole system, as can be seen in Tab.1. The oscillation frequency ratios can be seen in the frequency spectrum in Fig. 11.

Finally, the difference in angles between the movement of the leaf spring and the free end of the flexible cylinder is shown in Figs. 12 and 13. It should be noted that rigid and flexible displacements are not always in phase.

Regarding Case 05, see Fig. 12, the movement starts with a small difference, then, in the first synchronization range $5 < Vr < 11$, the movements are in phase. In the second region, they are clearly in anti-phase, reaching an angle difference of 180 degrees. These angle differences confirmed the first and third modes for this system, as illustrated in Fig.4 (g and i), respectively.

For the second position, Case 06, see Fig. 13, for $Vr < 11$, the movements are in phase. For $Vr > 11$ the anti-phase movement starts, which agrees with the beginning of the second synchronization. In Figs.4 (j and l), the modal shape confirms these phase differences.

From the amplitudes, frequencies, and phase analysis, it is possible to conclude that when the rigid and flexible body movements are coupled, there is no predominance of one or another mode of vibration. What happens is that the entire structure behaves differently, with its own modes of vibration and characteristic frequencies. The first mode of vibration

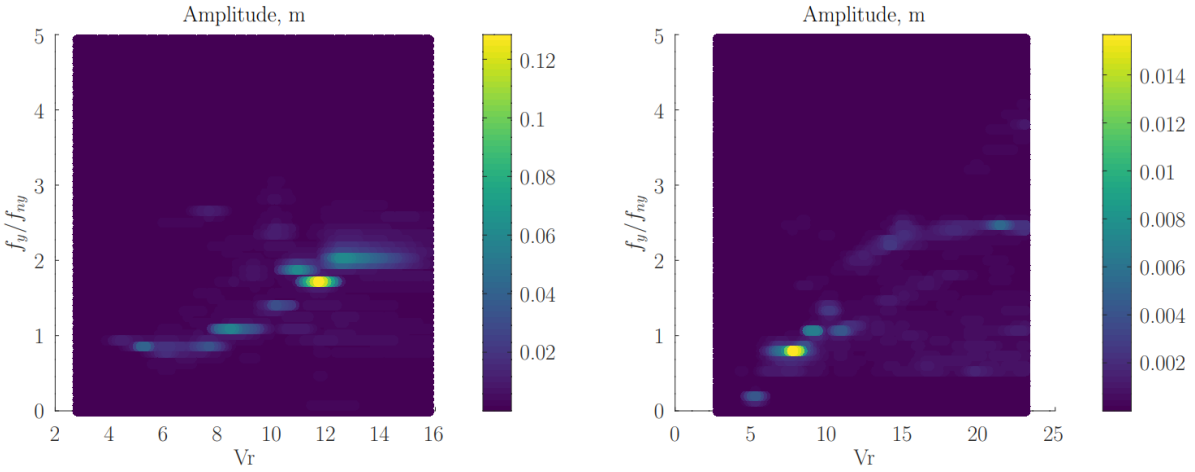

Figure 11. Frequency spectrum for the flexible cylinder with leaf spring at 0.64Hz(left) and 1Hz(right).

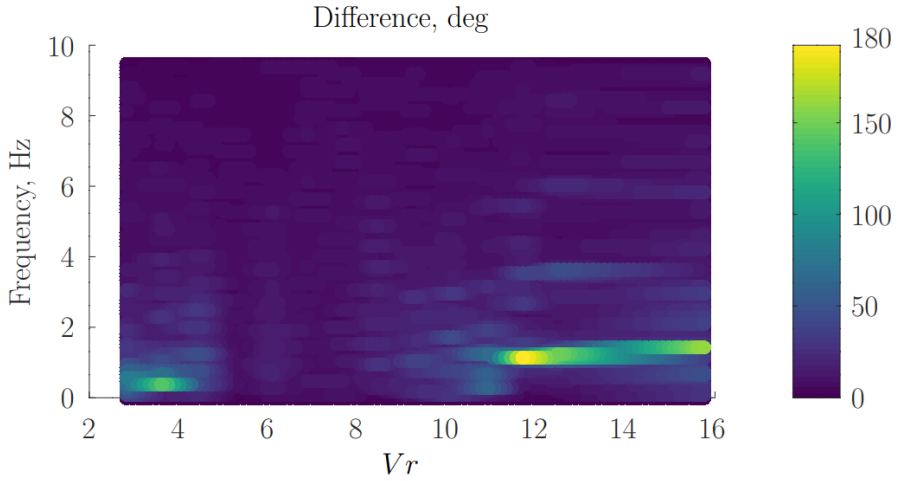

Figure 12. Phase map for Case 05.

occurs when the rigid and flexible displacements are in phase, near the first flexible natural frequency. The second mode is only for the flexible cylinder to vibrate at its first natural frequency in the inline direction. The third mode is rigid and flexible movements in anti-phase, vibrating in a frequency between the second flexible mode and the rigid frequency.

6. CONCLUSIONS

Flexible structures are characterized by the multimodal response to vibration. The modes of vibration are intrinsically related to the boundary conditions. The vortex-induced vibration response, when evaluated in a wide range of velocities, presents distinct synchronization regions, with modal co-existence in a peak frequency.

In this work, rigid and flexible cylinders were mounted on an elastic support, which regulates the stiffness value according to the length of its leaf springs. The rigid cylinder has shown a standard VIV response curve, with initial, upper and lower branches, with a maximum RMS amplitude of $0.6D$ in the cross-flow direction. The flexible champed-free cylinder has presented a jump to the upper branch region, with a maximum cross-flow amplitude of $1.1D$ in the first synchronization and $0.9D$ in the second synchronization.

When the coupled rigid-flexible modes are analyzed, the rigid amplitudes decrease drastically, and the synchronization ranges are shifted to higher velocities. The displacements of the flexible cylinder, otherwise, increase the amplitudes, reaching a peak of $1.6D$ in the first synchronization, when the rigid and flexible modes are in phase. When movements are in anti-phase, the maximum amplitude is 0.5D, vibrating at $1.2Hz$ for the longer span length and at a frequency about $1.4Hz$ for the shorter span length. Both leaf spring positions tested have shown similar amplitudes in the two synchronization regions found.

From the present experiments, it is possible to conclude that when rigid- and flexible-body modes are coupled, the amplitudes are similar regardless of the rigid-body stiffness, amplified in the first synchronization, and attenuated in the second one. Vibration frequencies are also different from the separated movements. The first synchronization is governed

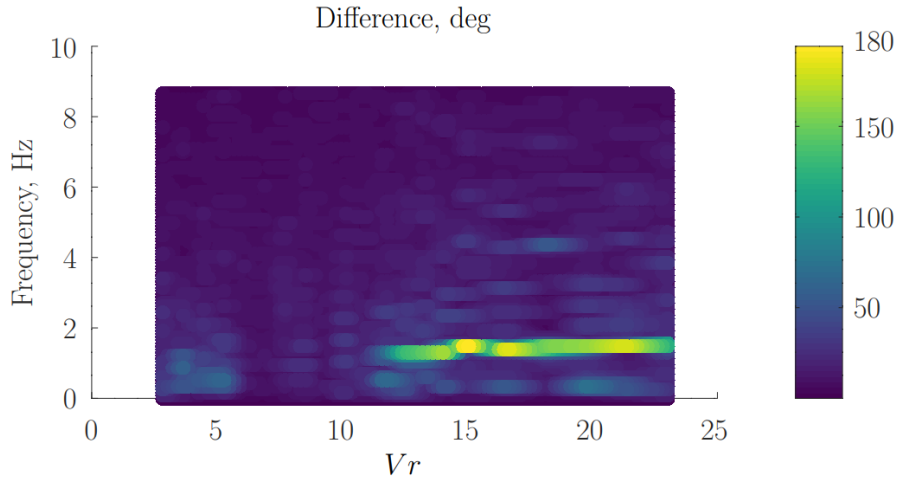

Figure 13. Phase map for Case 06.

by the flexible first-mode frequency, but the second synchronization vibrates at a frequency between the rigid and second modes of the flexible cylinder only.

Exploring these aspects contributes to advancing the understanding of VIV in flexible structures, especially when rigid and flexible modes are coupled, and enhances the predictive capabilities for practical applications in engineering and offshore structures. Future work will investigate a broader range of rigid body stiffness and flexible cylinder models.

ACKNOWLEDGEMENTS

The first author acknowledges Coordenação de Aperfeiçoamento de Pessoal de Nível Superior – Brazil (CAPES) for funding the PhD studies. The second, third and fourth authors acknowledge the Brazilian National Research Council (CNPq) for the grants 305945/2020-3, 314057/ 2021-8 and 307995/2022-4. The Sao Paulo Research Foundation (FAPESP) thematic project 'Nonlinear Dynamics Applied to Engineering Systems', process 2022/00770-0, is acknowledged.

REFERENCES

Franzini, G.R., Gonçalves, R.T., Pesce, C.P., Fujarra, A.L., Mazzilli, C.E., Meneghini, J.R. and Mendes, P., 2015. "Vortex-induced vibration experiments with a long semi-immersed flexible cylinder under tension modulation: Fourier transform and hilbert–huang spectral analyses". *Journal of the Brazilian Society of Mechanical Sciences and Engineering*, Vol. 37, pp. 589–599.

Franzini, G.R., Pereira, A.A., Fujarra, A.L. and Pesce, C.P., 2008. "Experiments on viv under frequency modulation and at constant reynolds numbers". In *International Conference on Offshore Mechanics and Arctic Engineering*. Vol. 48227, pp. 959–968.

Franzini, G.R., Pesce, C.P., Gonçalves, R.T., Mendes, P. and Fujarra, A., 2016. "Experimental investigations on vortex-induced vibrations with a long flexible cylinder. part ii: effect of axial motion excitation in a vertical configuration". In *Proceedings of the 11th International Conference on Flow-Induced Vibration*.

Franzini, G.R., Pesce, C.P., Gonçalves, R.T., Fujarra, A.L. and Pereira, A.A., 2014. "Concomitant vortex-induced vibration experiments: a cantilevered flexible cylinder and a rigid cylinder mounted on a leaf-spring apparatus". *Journal of the Brazilian Society of Mechanical Sciences and Engineering*, Vol. 36, pp. 547–558.

Fujarra, A.L.C., Leal, A.P., Carnier, R.M., Gonçalves, R.T. and Suzuki, H., 2023. "Validation of a low-cost imu for flow-induced vibration tracking in offshore systems". *Journal of the Brazilian Society of Mechanical Sciences and Engineering*, Vol. 45, No. 7, p. 356.

Govardhan, R. and Williamson, C., 2000. "Modes of vortex formation and frequency response of a freely vibrating cylinder". *Journal of Fluid Mechanics*, Vol. 420, pp. 85–130.

Khalak, A. and Williamson, C.H., 1999. "Motions, forces and mode transitions in vortex-induced vibrations at low mass-damping". *Journal of fluids and Structures*, Vol. 13, No. 7-8, pp. 813–851.

Pesce, C.P., Fujarra, A.L. and Kubota, L.K., 2006. "The hilbert-huang spectral analysis method applied to viv". In *International Conference on Offshore Mechanics and Arctic Engineering*. Vol. 47497, pp. 551–561.

Pesce, C.P. and Fujarra, A.L.C., 2000. "Vortex-induced vibrations and jump phenomenon: experiments with a clamped flexible cylinder in water". *International Journal of Offshore and Polar Engineering*, Vol. 10, No. 01.

Pesce, C. and Fujarra, A., 2005. "The super-upper branch viv response of flexible cylinders". In *BBVIV4, Conf Bluff Body*

Wakes and Vortex-Induced Vibrations, Santorini, Greece.
Williamson, C.H. and Govardhan, R., 2004. "Vortex-induced vibrations". *Annu. Rev. Fluid Mech.*, Vol. 36, pp. 413–455.